

Diversity of charge orderings in correlated systems

Konrad Jerzy Kapcia,^{1,2,*} Jan Barański,^{1,†} and Andrzej Ptok^{2,3,‡}

¹*Institute of Physics, Polish Academy of Sciences,
Aleja Lotników 32/46, PL-02-668 Warsaw, Poland*

²*Institute of Nuclear Physics, Polish Academy of Sciences,
ul. E. Radzikowskiego 152, PL-31-342 Kraków, Poland*

³*Institute of Physics, Maria Curie-Skłodowska University,
Plac M. Skłodowskiej-Curie 1, PL-20-031 Lublin, Poland*

(Dated: October 4, 2017)

The phenomenon associated with inhomogeneous distribution of electron density is known as a charge ordering. In this work, we study the zero-bandwidth limit of the extended Hubbard model, which can be considered as a simple effective model of charge ordered insulators. It consists of the on-site interaction U and the intersite density-density interactions W_1 and W_2 between nearest-neighbors and next-nearest neighbors, respectively. We derived the exact ground state diagrams for different lattice dimensionalities and discuss effects of small finite temperatures in the limit of high dimensions. In particular, we estimated the critical interactions for which new ordered phases emerge (laminar or stripe and four-sublattice-type). Our analysis shows that the ground state of the model is highly degenerated. One of the most intriguing findings is that the nonzero temperature removes these degenerations.

PACS numbers:

71.10.Fd — Lattice fermion models (Hubbard model, etc.),

71.45.Lr — Charge-density-wave systems,

64.75.Gh — Phase separation and segregation in model systems (hard spheres, Lennard-Jones, etc.),

71.10.Hf — Non-Fermi-liquid ground states, electron phase diagrams and phase transitions in model systems

Keywords:

extended Hubbard model, atomic limit, charge-order, stripes, long-range interactions, phase diagrams

I. FORMULATION OF THE PROBLEM

The solutions of the extended Hubbard model predicts an existence of the states with the inhomogeneous spatial distribution of electrons [1–9]. This phenomenon is known as the charge ordering and can be observed in variety of compounds, e.g., cuprates [10–13], multiferroics [14, 15] and other intensively studied materials [16–18]. The simplest example of such an order is an alternate modulation of electron concentration on the bipartite lattice. In such a setup one can distinguish two equivalent sublattices, where every site in each sublattice is occupied by the same number of particles. This is so-called two sublattice assumption. In more general systems in which longer-range interactions play an important role the two-sublattice solutions does not capture the full basis of charge ordered phases [19–23]. In order to properly describe these orderings one needs to take into account more than two inequivalent sites. The most conspicuous classes of such materials are those where laminar or stripe orderings appear, e.g., manganites [24, 25], cobaltites [26], and other transition-metal compounds [27].

The exact solution of the extended Hubbard model is still unknown, even in one dimension. A good testing field for approximate solutions would be results obtained

for simplified, but exactly solvable model (in arbitrary dimensions). The Hubbard model (without intersite interactions) has been exactly solved in one dimension [28, 29] and in the limit of infinite dimension [30–32]. Another approach is to neglect the hopping term instead of longer-range interactions. Similar conditions can be met in narrow band materials [3]. One of the main goals of the present work is to provide the exact solutions that can be compared with approximate results for more complex systems (such as models taking into account quantum fluctuations introduced by the hopping term).

In this work we investigate the extended Hubbard model in the atomic limit taking into account the next-nearest-neighbour density-density interactions. We assume that the mean-field solutions (with an exact treatment of the on-site terms) are contained within the four-sublattice system. This assumption is justified as long as we do not take into account interactions with longer range than the next-nearest neighbour. Phase diagrams in this approach are obtained for full range of model parameters. We note that the presented ground state solutions are exact for arbitrary dimensionality of the lattice. In a case of the high-dimension limit ($d \rightarrow +\infty$) we also present the effects associated with finite temperature. In addition, we discuss the qualitative differences of ordering range depending on dimensionality of the considered system.

The extended Hubbard model in the zero-bandwidth limit with interactions restricted to the second neighbors

* corresponding author; e-mail: konrad.kapcia@ifpan.edu.pl

† e-mail: jan.baranski@ifpan.edu.pl

‡ e-mail: aptok@mmj.pl

can be expressed as:

$$\hat{H} = U \sum_i n_{i\uparrow} n_{i\downarrow} + \frac{W_1}{2z_1} \sum_{\langle i,j \rangle_1} n_i n_j \quad (1)$$

$$+ \frac{W_2}{2z_2} \sum_{\langle i,j \rangle_2} n_i n_j - \mu \sum_i n_i,$$

where $c_{i\sigma}^\dagger$ denotes the creation operator of an electron with spin σ at the site i , $n_i = \sum_\sigma n_{i\sigma}$, $n_{i\sigma} = c_{i\sigma}^\dagger c_{i\sigma}$, U is the on-site density interaction, and W_1 and W_2 are the intersite density-density interactions between nearest neighbours (NNs) and next-nearest neighbours (NNNs), respectively. z_1 and z_2 are numbers of NNs and NNNs, respectively. μ is the chemical potential determining the total concentration n of electrons in the system by the relation $n = \frac{1}{L} \sum_i \langle n_i \rangle$, where $0 \leq n \leq 2$ and L is the total number of lattice sites. We inspect phase diagrams emerging from this model. The analyses are performed in the grand canonical ensemble.

Model (1) with neglected next-nearest interactions ($W_2 = 0$) was intensively studied using various methods. In particular, the exact solutions for a one-dimensional ($d = 1$) chain were obtained using the transfer-matrix method [33–35] or equations of motion and Green's function formalism [36–39]. The rigorous ground state phase diagrams as a function of μ were obtained for $W_2 = 0$ and $d \geq 1$ [40–42]. For a square lattice ($d = 2$) Monte Carlo simulations were performed [43, 44]. The model on the Bethe lattice was also analysed [45, 46]. The only known work beyond mean-field approaches for $W_2 \neq 0$ treats the model within the transfer-matrix method for $d = 1$ chain [47, 48] and the checker-board estimate with respect to lattice planes [40].

Using the mean-field method for alternate lattices it was shown that the system can exhibit several homogeneous charge-ordered phases as well as various phase separated states [49–52]. A case of $W_2 \neq 0$ within a mean-field approach was investigated in Refs. [51, 52]. However, these analyses were restricted to the two-sublattice assumption. This restriction is sufficient only for attractive W_2 , where there are no physical mechanisms supporting the four-sublattice type order. In the present work we perform the studies of the model for the full range of parameters including repulsive $W_2 > 0$. Our preliminary results only for $U < 0$ have been presented in Ref. [53]. One of the conclusions of the mentioned work was that the magnitude of on-site attractive U does not change the diagrams of the model qualitatively. Therefore, in the present work we mainly focus on repulsive U . We show that at particular values of $U > 0$ new phases emerge.

The mean-field expressions

The grand thermodynamic potential per site Ω_0 for model (1) in the grand canonical ensemble and in the

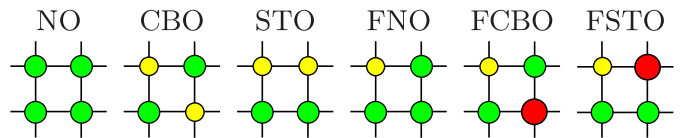


FIG. 1. Schematic representation of all possible homogeneous solutions for four-sublattice orderings at the ground state. Different sizes of dots correspond to different concentrations n_α ($\alpha = A, B, C, D$) in the sublattices. Note that each pattern can be realised in a few distinct forms (Tables I and II) due to specific concentrations of each site.

mean-field four-sublattice approximation at $T = 0$ can be expressed as

$$\Omega_0 = \langle \hat{H} \rangle / L = E_U + E_W + E_\mu, \quad (2)$$

where

$$E_U = \frac{1}{8} U [n_A(n_A - 1) + n_B(n_B - 1) + n_C(n_C - 1) + n_D(n_D - 1)], \quad (3)$$

$$E_W = \frac{1}{8} W_1 (n_A n_B + n_A n_D + n_B n_C + n_C n_D) + \frac{1}{4} W_2 (n_A n_C + n_B n_D), \quad (4)$$

$$E_\mu = -\frac{1}{4} \mu (n_A + n_B + n_C + n_D), \quad (5)$$

and n_α denotes the average number of particles in each sublattice $n_\alpha = \frac{4}{L} \sum_{i \in \alpha} \langle n_i \rangle$, $\alpha \in \{A, B, C, D\}$. In this work we adopted the convention that the NNNs for any site from A (B) sublattice are those and only those sites, which are located in C (D , respectively) sublattice.

For finite temperatures, the expressions given in Ref. [51] in the four-sublattice assumption takes the following forms. For n_α one gets

$$n_\alpha = \frac{2}{Z_\alpha} [\exp(\beta \mu_\alpha) + \exp(2\mu_\alpha - U)]. \quad (6)$$

For a grand canonical potential (per lattice site) one obtains:

$$\Omega = -\frac{1}{8} \sum_\alpha \Phi_\alpha n_\alpha - \frac{1}{4\beta} \sum_\alpha (\ln Z_\alpha), \quad (7)$$

where $\beta = 1/(k_B T)$ is inverted temperature, $\mu_\alpha = \mu - \Phi_\alpha$, and

$$Z_\alpha = 1 + 2 \exp \beta \mu_\alpha + \exp \beta (2\mu_\alpha - U), \quad (8)$$

$$\Phi_A = \frac{1}{2} W_1 (n_B + n_D) + W_2 n_C, \quad (9)$$

$$\Phi_B = \frac{1}{2} W_1 (n_A + n_C) + W_2 n_D, \quad (10)$$

$$\Phi_C = \frac{1}{2} W_1 (n_B + n_D) + W_2 n_A, \quad (11)$$

$$\Phi_D = \frac{1}{2} W_1 (n_A + n_C) + W_2 n_B. \quad (12)$$

II. PHASE DIAGRAMS AT HIGH DIMENSIONS

In this paragraph we present the ground state solutions of model (1) in the limit of high dimensions i.e. $d \rightarrow +\infty$

(or equivalently the limit of large coordination number: $z_1 \rightarrow +\infty$ and $z_2 \rightarrow +\infty$) and compare them to the results obtained for finite temperatures. We present the phase diagrams for fixed chemical potential as well as for fixed total electron concentration. In the following analyses $|W_1|$ is used as the energy unit. The solutions for repulsive $W_1 > 0$ and attractive $W_1 < 0$ are analysed separately.

In our system only six (inequivalent) homogeneous phases can occur at $T = 0$. They are determined by the relations between n_α 's (but several equivalent solutions exist due to cyclic change of sublattices indexes α). For intuitive understanding of rather complicated phase diagrams each pattern is marked with adequate abbreviation. Nonordered (NO), checker-board-ordered (CBO), and stripe-ordered (STO) phases can be realized using two sublattices, while the letter ‘‘F’’ (in the names of the FNO, FCBO, and FSTO phases) indicates that these types of ordering requires the four-sublattice assumption. All these phases are schematically depicted in Fig. 1. Each pattern can be realised in a few distinct forms depending on specific electron concentrations on each sublattice (cf. Tables I and II). Table I also contains the degeneracy of the ground state solutions (including charge- and spin- degrees of freedom).

A. Analysis for fixed chemical potential for repulsive W_1

First, we focus on the case of repulsive $W_1 > 0$. We discuss the qualitative changes of a phase diagrams with respect to on-site Coulomb interaction (U) as a function of chemical potential and next-nearest neighbour inter-site interactions (W_2). Below we present phase diagrams for a few representative on-site interactions, where qualitative differences occur. The diagrams are plotted for a full range of NNN interaction W_2 and shifted chemical potential $\bar{\mu}$ ($\bar{\mu} = \mu - \frac{1}{2}U - W_1 - W_2$). Notice that the model exhibits the particle-hole symmetry and thus all phase diagrams are symmetric towards $\bar{\mu} = 0$ (or $n = 1$) with $n_\alpha \longleftrightarrow 2 - n_\alpha$ transformation if one changes $\bar{\mu} \longleftrightarrow -\bar{\mu}$ (or $n \longleftrightarrow 2 - n$). The qualitative changes of phase diagrams occur at $U = 0.00$, $U = 0.50|W_1|$, and $U = 1.00|W_1|$. All possible phases (within the four-sublattice assumption) are collected in Table I. Their grand canonical potentials Ω_0 are calculated from Eqs. (2)–(5) and the phase with the lowest Ω_0 for given model parameters is determined.

It is rather intuitive that the attractive on-site interactions favours double occupancy and only phases with empty and doubly occupied states (i.e., the NO_0 (0000), CBO_2 (2020), STO_2 (2200), and FNO_2 (2000) phases) are stable for $U < 0$ (the numbers in the brackets denote the concentrations in sublattices ($n_A n_B n_C n_D$)). Changing the sign of U leads to the appearance of new phases with single occupied sites. These states can be considered as intermediate phases emerging from boundaries, e.g.,

TABLE I. The definitions of phases ($d \leq 3$) or elementary blocks ($d = 1, 2$) occurring in the ground state for total $n \leq 1$. Notation: 2 – doubly occupied site, 0 – empty site, 1 – singly occupied site. The degeneration $d_c \times d_s$ of the elementary blocks (equal to the degeneration of the ground state for $d \rightarrow +\infty$ limit) and degeneration $D_c \times D_s$ of the ground state phases constructed from the corresponding blocks for $d = 2$ ($L = N^2$) is given (with respect to charge- and spin- degrees of freedom).

Phase	n_A	n_B	n_C	n_D	$d_c \times d_s$	$D_c \times D_s$
NO_0	0	0	0	0	1×1	1×1
NO_1	1	1	1	1	1×16	1×2^L
CBO_1	1	0	1	0	2×4	$2 \times 2^{L/2}$
CBO_2	2	0	2	0	2×1	2×1
STO_1	1	1	0	0	4×4	$4 \times 2^{L/2}$
STO_2	2	2	0	0	4×1	4×1
FNO_1^a	1	0	0	0	4×2	$2^{N/2+2} \times 2^{L/4}$
FNO_2^a	2	0	0	0	4×1	$2^{N/2+2} \times 1$
FNO_3^a	1	1	1	0	4×8	$2^{N/2+2} \times 2^{3L/4}$
FCBO	2	0	1	0	4×2	$4 \times 2^{L/4}$
FCBO^b	2	1	0	1	4×4	$4 \times 2^{L/2}$
FSTO^a	2	1	0	0	8×2	$2^{N/2+2} \times 2^{L/4}$
$\text{FSTO}^{a,b}$	2	1	1	0	4×4	$2^{N/2+2} \times 2^{L/2}$

^a The long-range charge-order is ‘‘reduced’’ in the phase constructed from this elementary blocks in $d = 1, 2$.

^b This phase constructed from this elementary block does not occur in the ground state.

from boundary between NO_0 (0000) and FNO_2 (2000) phases the intermediate FNO_1 (1000) phase emerges. A Similar case occurs on the other side of the FNO_2 phase region, where for $U > 0$ the FSTO (2100) phase appears as an intermediate one between the FNO_2 and STO_2 (2200) phases. In such conditions the FNO_2 phase is sandwiched between two intermediate growing phases.

The qualitative changeover occurs for on-site energy $U = 0.50|W_1|$. For this value of interaction two electrons occupying one site in the FNO_2 phase can be separated to form the stripe-ordered STO_1 (1100) phase and thus for larger U the STO_1 phase is stable. We note that additional two phases (the FNO_3 (1110) and NO_1 (1111) phases) without double occupied sites emerge on boundaries around $W_2 = 0.5|W_1|$ and $-0.25|W_1| < \bar{\mu} < 0$. For $U > 0.5|W_1|$ the FNO_3 and NO_1 phases occurs in finite range of model parameters. With further increasing of U the region of the FCBO (2010) phase shrinks. The region of this phase occurrence at $U = 1.00|W_1|$ is reduced to a single point. For $U > 1.00|W_1|$ the NO_1 – CBO_1 transitions appears and for larger values of U the diagram does not change, qualitatively. Remarkably, the FCBO phase exists only for define range of on-site interaction, while the FSTO phase is present for arbitrarily large U .

Notice that all boundaries between ground state phases in Fig. 2 are discontinuous (first order transitions associated with discontinuous change of at least one of the n_α 's). At the boundaries two phases possess the same energy. If two phases coexist in the system the inter-

increases as L^γ with $\gamma < 1$ (where L is the number of lattice sites) the contribution of the interface energy to the total energy of the system vanishes in the thermodynamic limit. In such a case, the macroscopic phase domains will be formed. A formation of these regions with different orderings is known in physics as the (macroscopic) phase separation (PS) (the only one possible type of a coexistence of two phases in $d \rightarrow +\infty$ limit). Otherwise, for $\gamma > 1$ the formation of the interfaces is disfavoured and the co-existence of the phases is not allowed in the system. In such situation, even though both phases have the same energy, only one type of the ordering is realized in all volume of the system. We note, however, that we did not find such behaviour in the considered model.

Effects of finite temperatures (fixed μ)

So far we considered the ground state ($T = 0$), where all phase transitions are associated with a discontinuous change of at least one sublattice concentration n_α . In this subsection we discuss the influence of a finite temperatures on phase transitions slightly above the ground state. The phases are found by numerically solving the set of four self-consistent equations in a form of (6) and finding the solution corresponding to the lowest Ω determined by (7).

For attractive W_2 the behaviour of the system does not change qualitatively at small temperatures, and all phase transitions remain first-order. At critical $W_2 = 0$ the order of all transitions changes into the second one. A more complex situation occurs for repulsive W_2 . Our analysis shows that all ground state FNO–STO boundaries (namely, (2000)–(2200), (1000)–(1100), and (1110)–(1100)) and boundary lines which are not dependent on the chemical potential (horizontal lines in Fig. 2) remain first-order. All other transitions for $W_2 > 0$ are second-order at small $T > 0$. At finite temperature, the FNO phases are no longer stable, and they are converted into FCBO phases, i.e. $(n_A 000)_{T=0} \rightarrow (n_A n_B n_C n_B)_{T>0}$. As a result the ground state FNO₁–FNO₂ ((1000)–(2000)) and FNO₂–FCBO ((2000)–(2010)) boundaries no longer exist at $T > 0$ (Fig. 2(b)). The similar situation takes place for the CBO₁–CBO₂ boundary for $W_2 = 0$ [52].

Additionally, we noticed that finite temperature, for small $W_2 > 0$, gives rise to checker-board orderings between NO and FNO phases. Namely, NO–FNO boundaries change into the NO–CBO–FNO sequence of second-order transitions with changing chemical potential. In particular, the following sequences emerge: NO₀–CBO₂–FNO₂, NO₀–CBO₁–FNO₁, FNO₃–CBO₁–NO₁ (cf. Ref. [53] for the $U < 0$ case). For larger values of W_2 , the CBO phases are absent and only second-order transitions between corresponding NO and FNO phases occur.

B. Analysis for fixed electron concentration for repulsive W_1

Here we consider the mutual relations between homogeneous phases and phase separated states for fixed total concentrations n . To do this one needs to first establish which homogenous phases have the lowest energies and then compare them to the energies of phase separated states. The first step is illustrated in Fig. 3, which presents the phase diagrams as a function of electron concentration. Each rectangular region of the diagrams is labeled by the abbreviation of homogeneous phase with the lowest free energy. The meaning of each label is given in Table II. The free energy per site of homogeneous phases at $T = 0$ within the mean-field approximation can be obtained as $f_0 = UD_{occ} + E_W$, where E_W is expressed by Eq. (4). The double occupancy D_{occ} and n_α are also collected in Table II. On the vertical boundaries (for commensurate particle fillings $n = i/4$, $i = 1, 2, 3, 4$) the homogeneous phases occur. These phases can be read from Table I and Fig. 2). For $n = 1/2$ on the boundary between FSTO_D and FSTO_F regions the STO₁ phase occurs (Fig. 3(f)). On the horizontal boundaries the phases from both neighboring regions have equal energies, and they coexist.

So far we labelled only homogenous phases with the lowest energies. The comparison of them with the phase separated states shows that for $W_2 < 0$ the homogeneous phases are unstable (i.e. $\partial\mu/\partial n < 0$) and thus only the PS states are present. These regions in Fig. 3 are marked by a slantwise pattern. The obvious exclusion from this pattern occurs for vertical boundaries between two types of PS states where homogenous phases are stable below $W_2 = 0$. We determined that at $T = 0$ and $W_2 \geq 0$ homogenous phases and PS states have the same energy. The corresponding PS states in each region of Fig. 3 are given in the last column of Table II. We would like to emphasize that the system cannot be simultaneously in a homogenous phase and a PS state. Thus even though energies of PS states and homogeneous phases at $T = 0$ are equal, the system must “choose” one of the solutions. This type of degeneracy is removed by the finite temperature. The free energies of the (macroscopic) PS states are calculated from the expression $f_{PS} = mf_+(n_+) + (1-m)f_-(n_-)$, where $f_\pm(n_\pm)$ are free energies of separating homogeneous phases and $m = (n - n_-)/(n_+ - n_-)$ is a fraction of the system which is occupied by the phase with concentration n_+ .

Additionally, we note that for fixed W_2 transitions between homogeneous phases (horizontal lines in Fig. 3) are associated with continuous change of sublattice concentrations, whereas for fixed n (vertical boundaries) the sublattice concentrations change discontinuously (at commensurate fillings only at points indicated by square symbols in Fig. 3). All transitions between the phases exhibit discontinuous change of chemical potential.

Notice also that mean-field results presented in Fig. 3 ($W_1 > 0$) are coincided with some exact results obtained

TABLE II. The definitions of homogeneous phases which can occur in the mean-field ground state of the model as a function of n and ranges $[n_s, n_f]$ of electron concentration where the phases are defined properly. For each phase the double occupancy D_{occ} defined as $D_{occ} = \frac{1}{L} \sum_i \langle n_{i\uparrow} n_{i\downarrow} \rangle$ is also calculated (exact result for $d \rightarrow +\infty$). At the last column the corresponding phase separated states are mentioned (cf. Table I).

Phase	n_A	n_B	n_C	n_D	D_{occ}	n_s	n_f	PS state
NO _A	n	n	n	n	$n/2$	0	2	NO ₀ /NO ₂
NO _B	n	n	n	n	0	0	1	NO ₀ /NO ₁
CBO _A	$2n$	0	$2n$	0	$n/2$	0	1	NO ₀ /CBO ₂
CBO _B	$2n$	0	$2n$	0	0	0	1/2	NO ₀ /CBO ₁
CBO _C	$2n$	0	$2n$	0	$n - 1/2$	1/2	1	CBO ₁ /CBO ₂
CBO _D	1	$2n - 1$	1	$2n - 1$	0	1/2	1	CBO ₁ /NO ₁
STO _A	$2n$	$2n$	0	0	$n/2$	0	1	NO ₀ /STO ₂
STO _B	$2n$	$2n$	0	0	0	0	1/2	NO ₀ /STO ₁
STO _C	$2n$	$2n$	0	0	$n - 1/2$	1/2	1	STO ₁ /STO ₂
STO _D	1	$2n - 1$	$2n - 1$	1	0	1/2	1	STO ₁ /NO ₁
FNO _A	$4n$	0	0	0	$n/2$	0	1/2	NO ₀ /FNO ₂
FNO _B	$4n$	0	0	0	0	0	1/4	NO ₀ /FNO ₁
FNO _C	$4n$	0	0	0	$n - 1/4$	1/4	1/2	FNO ₁ /FNO ₂
FCBO _A	2	0	$4n - 2$	0	$n/2$	1/2	1	FNO ₂ /CBO ₂
FCBO _B	2	0	$4n - 2$	0	$n - 1/2$	3/4	1	FCBO/CBO ₂
FCBO _C	2	0	$4n - 2$	0	1/4	1/2	3/4	FNO ₂ /FCBO
FCBO _D	1	0	$4n - 1$	0	0	1/4	1/2	FNO ₁ /CBO ₁
FCBO _E	1	0	$4n - 1$	0	$n - 1/2$	1/2	3/4	CBO ₁ /FCBO
FCBO _F	1	$4n - 2$	1	0	0	1/2	3/4	CBO ₁ /FNO ₃
FCBO _G	1	$4n - 3$	1	1	0	3/4	1	FNO ₃ /NO ₁
FSTO _A	2	$4n - 2$	0	0	$n/2$	1/2	1	FNO ₂ /STO ₂
FSTO _B	2	$4n - 2$	0	0	1/4	1/2	3/4	FNO ₂ /FSTO
FSTO _C	2	$4n - 2$	0	0	$n - 1/2$	3/4	1	FSTO/FSTO ₂
FSTO _D	1	$4n - 1$	0	0	0	1/4	1/2	FNO ₁ /STO ₁
FSTO _E	1	$4n - 1$	0	0	$n - 1/2$	1/2	3/4	STO ₁ /FSTO
FSTO _F	1	1	$4n - 2$	0	0	1/2	3/4	STO ₁ /FNO ₃

for a one-dimensional chain at $T = 0$ and arbitrary n . In particular, the mean-field approximation used in the present work predicts properly the values for (free) energy, double occupancy correlation function, and nearest- and next-nearest two-point correlation functions [38, 48]. Ref. [38] predicts also that at $T = 0$ and for $W_2 = 0$ ($W_1 > 0$) the long-range checker-board order exist in the following range of model parameters: (i) $0 < U < W_1$ and $1/2 < n < 1$, (ii) $U > 0$ and $n = 1/2$, (iii) $U < W_1$ and $n = 1$. We found the similar behaviour for $W_2 > 0$ in the FCBO_B and FCBO_E regions (Fig. 3(b)–(d)), where the long-range checker-board order is expected for $d = 1$ and $d = 2$ at zero temperature. For (a) $W_1 > 0$ and $W_2 < 0$ as well as (b) $W_1 < 0$ and any W_2 at $T = 0$ and $d = 1, 2$ the macroscopic phase separation involving the checkerboard order would occur (for incommensurate fillings).

Influence of finite temperatures (fixed n)

For $W_2 < 0$ the finite temperature does not change qualitative behavior of the system and the PS are still stable. For $W_2 \geq 0$, infinitely small $T > 0$ breaks the energy equality between homogeneous phases and PS states and only one of them is stable. Namely, the PS states be-

tween FNO and STO phases emerge at the regions filled by grating pattern for $W_2 > 1/2$, whereas in empty regions in Fig. 3 the homogeneous phases are favoured. For $W_2 = 0$ only the homogeneous CBO phases are present. Remarkably, the regions of the PS states occurrence (slantwise and grating patterns) are separated by homogeneous phases (empty regions) at $T > 0$. The stability of the PS states at $T > 0$ in these regions is a result of discontinuous transitions with changing $\bar{\mu}$, e.g., Refs. [51, 52]. Note that at $T > 0$ the separating homogeneous phases are the phases with particle concentrations different than those at the ground state, and they can be determined by the so-called Maxwell's construction (cf., e.g., Ref. [51]).

Due to the fact that at finite temperatures sublattice concentrations change continuously for fixed $W_2/|W_1|$ (vertical lines between nonfilled regions in Fig. 3) only boundaries between different types of phases still exist. Boundaries between the same type of phases (e.g., FCBO_B–FCBO_E) are smeared out. We also note that $T > 0$ transforms all FNO phases into FCBO phase. Therefore, ground state FNO–FCBO boundaries are also smeared (vanish) at nonzero temperatures. One should be aware of the type of phase occurring at commensurate filling (at vertical boundaries of diagrams in Fig. 3). For example, at the ground state FCBO_B–FCBO_E bound-

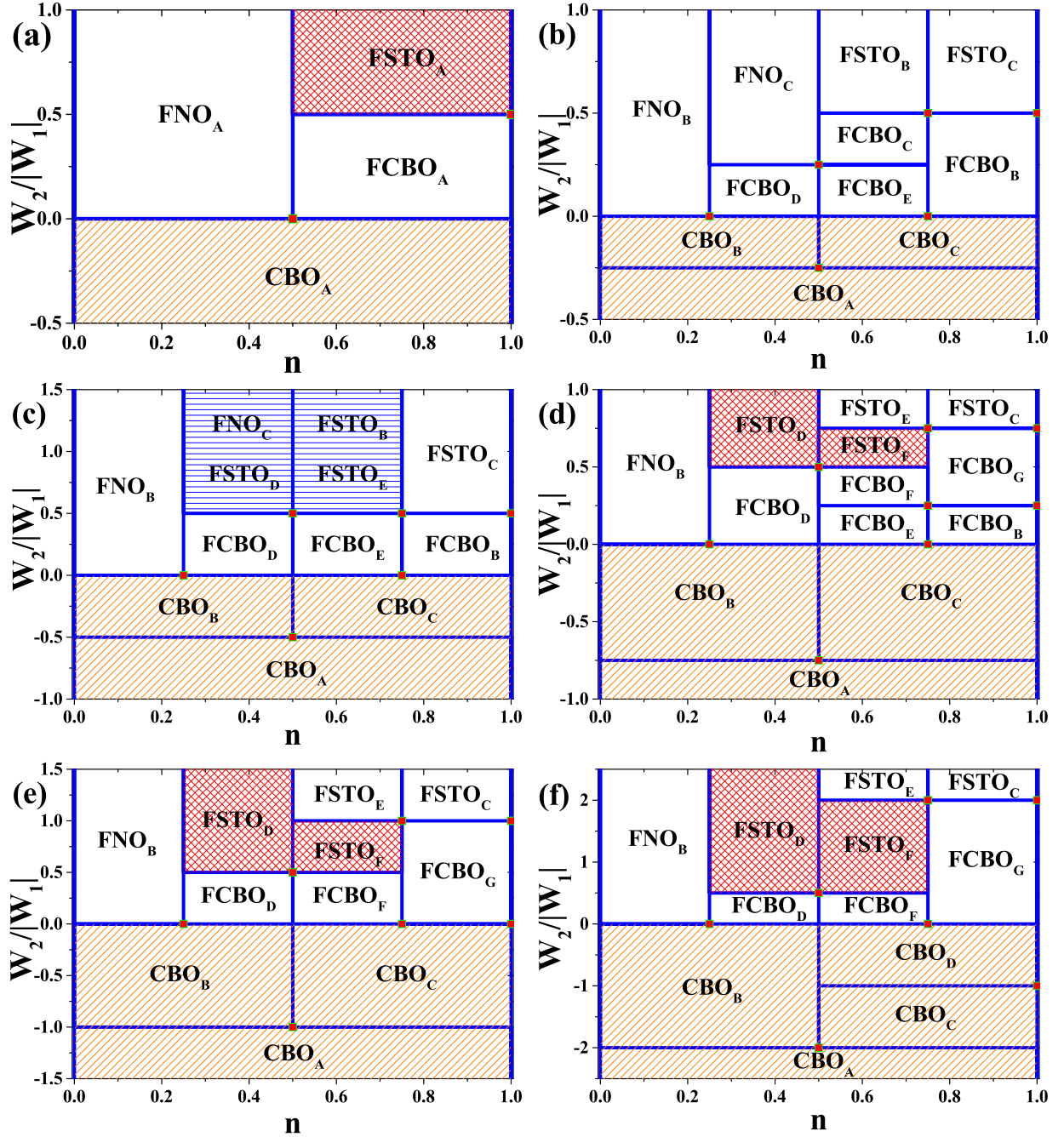


FIG. 3. (Color online) Ground state phase diagrams as a function of electron concentration for $W_1 > 0$ and (a) $U/|W_1| \leq 0.00$, (b) $U/|W_1| = 0.25$, (c) $U/|W_1| = 0.50$, (d) $U/|W_1| = 0.75$, (e) $U/|W_1| = 1.00$, (f) $U/|W_1| = 2.00$. Each rectangular region of the diagrams is labelled by the name of homogeneous phase with the lowest free energy (cf. Table II). In regions filled by slantwise pattern the corresponding PS state is stable at $T = 0$ and at infinitesimally small $T > 0$. In regions filled by grating pattern the homogeneous phase and PS state have equal free energies at $T = 0$ whereas the PS state is stable at infinitesimally small $T > 0$. In nonfilled regions the homogeneous phase and PS state have equal free energies at $T = 0$ whereas the homogeneous phase is stable at infinitesimally small $T > 0$. At vertical boundaries only the homogeneous phases occur (cf. Table I and Fig. 2). The rectangular points indicate discontinuous transitions at commensurate fillings.

ary (Fig. 3(c)) the FCBO phase occur and thus this boundary vanishes at $T > 0$. The situation changes for FCBO_D – FCBO_E and FCBO_D – FCBO_F boundaries (e.g. Fig. 3(d)), where for $n = 1/2$ the CBO_1 phase occurs

at $T = 0$. As a result at small $T > 0$ the FCBO – CBO – FCBO sequence of transitions with changing n is present. For the ground state FNO_C – FSTO_B boundary (Fig. 3(b)), the FNO_2 phase is stable at $n = 1/2$ and

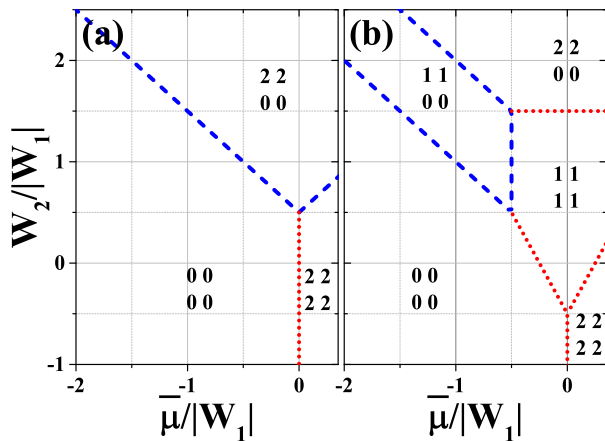


FIG. 4. (Color online) Ground state phase diagrams as a function of chemical potential for $W_1 < 0$ and (a) $U/|W_1| \leq 0$, (b) $U/|W_1| > 0$ ($\bar{\mu} = \mu - \frac{1}{2}U - W_1 - W_2$). Each region is labelled by electron concentrations in each sublattice: $(\begin{smallmatrix} n_A & n_B \\ n_D & n_C \end{smallmatrix})$ (cf. Table I). Dashed lines denote infinite degeneracy but not macroscopic, whereas dotted lines indicate finite degeneracy (at the boundaries for $d = 2$).

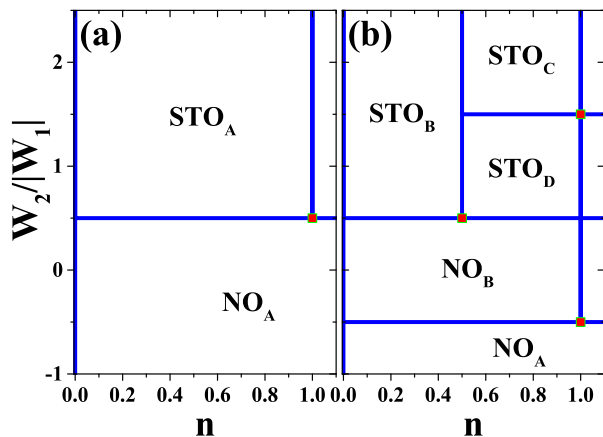


FIG. 5. (Color online) Ground state phase diagrams as a function of electron concentration for $W_1 < 0$ and (a) $U/|W_1| \leq 0$, (b) $U/|W_1| > 0$. Each rectangular region of the diagrams is labelled by the name of the homogeneous phase with the lowest free energy (cf. Table II). In all regions the corresponding PS states are stable at $T = 0$ and at infinitesimally small $T > 0$ (excluding vertical boundaries). The rectangular points indicate discontinuous transitions at commensurate fillings (cf. Fig. 2).

thus only the FCBO–FSTO transition occurs at finite T . By using the scheme shown one can analyze each of the ground state boundary at $n = i/4$ ($i = 1, 2, 3, 4$). One concludes that all ground state boundaries at $n = 1/4$ and $n = 3/4$ between homogeneous phases are smeared out at $T \neq 0$, whereas all those for $n = 0$ and $n = 1$ remain. For $n = 1/2$ only the ground state FNO_A–FCBO_A (Fig. 3(a)) and FNO_C–FCBO_C (Fig. 3(b)) vanishes at small finite T .

Finally, let us comment on transitions with changing $W_2/|W_1|$ for fixed n . All horizontal ground state boundaries, for $W_2 \neq 0$ remain discontinuous at $T > 0$. At the specific case of $W_2 = 0$ the CBO–FCBO and CBO–FNO boundaries are second order at nonzero temperatures (cf. also Ref. [53]). Moreover, the ground state CBO_A–CBO_B and CBO_A–CBO_C boundaries vanish at any finite T for $W_2 = 0$ (cf. Refs. [49, 51, 52]).

C. The case of attractive W_1

To provide the full picture of the system ground state we present results obtained for the attractive nearest-neighbour interaction ($W_1 < 0$).

This case is less complex than a case of W_1 as the qualitative behaviour of the system is not dependent on a magnitude of the on-site interaction (only the sign of U is relevant). For attractive W_1 only possible phases are either nonordered or stripe-ordered (STO) phases. In the case of $U < 0$ only phases with empty or double-occupied sites are realized (Fig. 4(a)), whereas for $U > 0$ the phases with single-occupied sites emerge (Fig. 4(b)). All phase boundaries are discontinuous. The above behaviour of the system is preserved also at small, but finite temperatures.

Similarly to the previous analyses, in Fig. 5 we present the phase diagrams as a function of concentration n . In this case the corresponding PS states (cf. Table II) possess lower energies than homogeneous phases in the full range of the model parameters (excluding vertical boundaries in Fig. 5). The attractive W_2 favours the PS states between nonordered phases, whereas repulsive W_2 gives rise to PS states involving various STO phases. Homogeneous phases on the vertical boundaries ($n = i/2$, $i = 1, 2$) can be read from Fig. 4 and Table I. On the horizontal boundaries the PS states from both neighboring regions have equal energies and they coexist. Moreover, at infinitesimally $T > 0$ the diagrams do not change and the PS states still occur.

III. LOW DIMENSIONAL SYSTEMS

So far we have discussed the mean-field solutions of the model, which is an exact theory in high dimensions (formally $d \rightarrow +\infty$, $z_n \rightarrow +\infty$) [54–56]. In this section we discuss the qualitative behavior of lower dimension systems, which fulfill the four-sublattice restriction. In particular, we consider the 1D chain, 2D square (SQ) lattice, and 3D base-centered cubic (BCC) lattice. For the 3D one we choose the BCC lattice because (unlike simple cubic or face-centered cubic lattices) it can be divided into four equivalent sublattices.

A set of four sublattice concentrations ($n_A n_B n_C n_D$) defines an elementary block. These blocks can be grouped in types. All blocks of a given type can be obtained by a cyclic change of sublattice indices, e.g., the

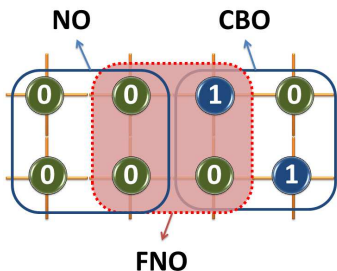


FIG. 6. (Color online) Schematic illustration of *nonmixing* block alignment in $d = 2$. Note that the FNO block at the interface between the NO and CBO phases emerge (shadow, dotted line). For $W_2/|W_1| < 0$ the FNO block does not yield the minimal energy.

FCBO type consists of four different elementary blocks, namely [(2010), (0201), (1020), (0102)]. Any elementary block of a ground state configuration must be among those that yield the minimal energy when extended periodically [40, 57–60]. In other words, in a construction of a $T = 0$ diagram as a function of $\bar{\mu}$ only elementary blocks with the lowest energy and periodic configurations obtained from them play a role. The grand canonical potentials of such states at $T = 0$ are equal to the potentials of mean-field phases determined from Eqs. (2)–(5) and collected in Table I. Thus the structure of the ground state diagrams presented in Figs. 2 and 4 remains unchanged in lower dimensions, but the properties of the system at the boundaries and inside given regions can change.

Let us look closely at conditions at which at least two phases (elementary blocks) have equal energies, i.e., at the boundaries between regions on the phase diagrams as a function of chemical potential. In dimensions $d \geq 3$ any two elementary blocks of different phases can not be mixed with each other. In lower dimensions $d < 3$ this mixing become possible and additional degeneracy appears. Generally, we can classify three types of phase boundaries with respect to elementary blocks mixing:

- (i) *Nonmixing case.* In this case on the boundaries between two phases the state of the system can be constructed by periodical repetition of only one type of elementary block. In other words elementary block of one type cannot be aligned next to a block of a different type. As an example of such a situation let us consider the $\text{NO}_0\text{-CBO}_1$ boundary. The elementary blocks of these phases are respectively $\begin{smallmatrix} 0 & 0 \\ 0 & 0 \end{smallmatrix}$ and $\begin{smallmatrix} 1 & 0 \\ 0 & 1 \end{smallmatrix}$. In Fig. 6 we show that if such blocks would be aligned next to each other the region with block $\begin{smallmatrix} 0 & 1 \\ 0 & 0 \end{smallmatrix}$ would always be created that does not yield the minimal energy. In such a case even though both phases possess equal energies the ground state cannot be built of the composition of them, but it must “choose” one of the solutions. Then a coexistence of the phases can be realized only on a macroscopic level and only if

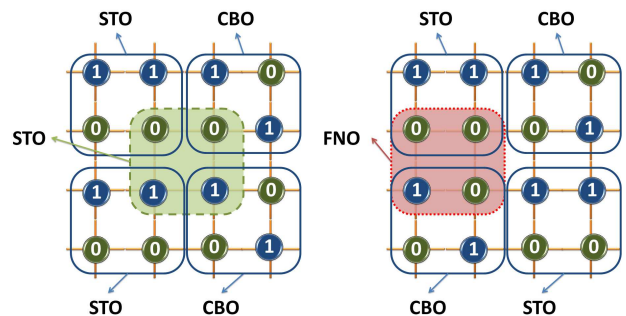


FIG. 7. (Color online) Schematic illustration of *partial-mixing* block alignments in $d = 2$ at the STO–CBO interface. In the left panel an allowed block orientation is shown (at the interfaces the STO or CBO blocks emerge). In the right panel a forbidden configuration is present, where in addition the FNO blocks emerge at the interface.

the contribution of the domain wall energy vanishes in the thermodynamical limit (the so-called macroscopic phase separation). Such types of boundaries at $d = 2$ are denoted by dotted lines in Figs. 2 and 4. At the boundaries the degeneracy is finite (modulo spin).

- (ii) *Partial mixing.* In Figs. 2 and 4 dashed-lines denote boundaries at which elementary blocks of different types can be aligned next to each other, but not arbitrarily (at $d = 2$). Some restrictions on a block’s configuration remains. An example of this type of the boundary occurs between the CBO_1 and STO_1 phases (see Fig. 7). We notice that if $\begin{smallmatrix} 1 & 0 \\ 0 & 1 \end{smallmatrix}$ and $\begin{smallmatrix} 1 & 1 \\ 0 & 0 \end{smallmatrix}$ blocks are aligned next to each other (in a given direction) we cannot find any region built of elementary blocks which does not belong to one of the phases with minimal energy (CBO_1 or STO_1). Specifically, it means that every column (or row) of blocks has to be purely built of one type of elementary blocks, whereas blocks can be freely aligned in rows (or columns). We note that opposed to non-mixing regime here we get microscopical mixing of each phase, but some macroscopic ordering remains as rows (or columns) are build of one type of elementary blocks. At such boundaries degeneracy Γ of the system is infinite but not macroscopic (modulo spin), i.e., it increases with size of the system (i.e., with L) lower than bA^L (where b and A are some fixed numbers; $0 < A < 3$) (entropy per site in the thermodynamic limit $s = \lim_{L \rightarrow +\infty} \frac{1}{L} \ln \Gamma$ is zero). Such boundaries at $d = 2$ are denoted by dashed lines in Figs. 2 and 4.
- (iii) *Full mixing.* Solid lines in Fig. 2 denote boundaries at which elementary blocks of neighboring regions can be aligned freely without any restrictions for $d = 2$ (macroscopic degeneration). As an example one can consider the $\text{FCBO}\text{-CBO}_1$ boundary; see Fig. 8. In this case the system is micro-

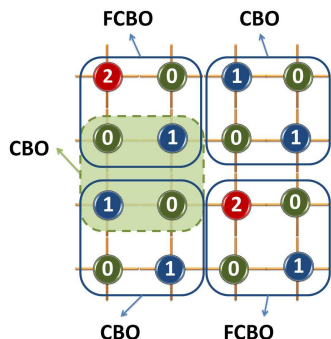


FIG. 8. (Color online) Schematic illustration of *full-mixing* block alignment in $d = 2$. All building blocks at the interface between the CBO and FCBO phases are blocks of one of these mixing phases. An exemplary block at the interface is denoted by the shadow (dashed line).

scopically mixed and therefore no macroscopic orderings are present. This type of boundaries at $d = 2$ is denoted by solid lines in Figs. 2. At such boundaries degeneracy Γ is infinite and macroscopic (modulo spin), i.e., it increases faster than bA^L (entropy per site in the thermodynamic limit $s = \lim_{L \rightarrow +\infty} \frac{1}{L} \ln \Gamma$ is finite).

For $d = 1$ the boundaries with infinite degeneration in Figs. 2 and 4 (dashed and solid lines) are macroscopically degenerated. In such a dimensionality of the system there is no *partial-mixing* at the boundaries.

Away from boundaries, in regions filled by the slantwise pattern in Fig. 2, two configurations of elementary blocks of the same phase can be mixed with each other, but arbitrarily. This situation is similar to a case of the *partial mixing* at phase boundaries. In low dimensions ($d = 1, 2$) mixing of the same type of elementary blocks but in different configurations (e.g. $\begin{smallmatrix} 2 & 0 \\ 1 & 0 \end{smallmatrix}$ and $\begin{smallmatrix} 1 & 0 \\ 2 & 0 \end{smallmatrix}$) leads to increased disorder in contrary to $d = 3$ case, where one configuration is present in whole system. Analogously to *partial mixing*, in the discussed cases every column (row) of blocks have to be purely built of elementary blocks in the same configurations, but blocks can vary from row to row (column to column), cf. Fig. 7. The ground state for $d = 2$ marked by the slantwise pattern in Fig. 2 has infinite degeneration, but it is not macroscopic (cf. Table I). For $d = 1$ the degeneracy in these regions is macroscopic.

To reach the situation, where in these regions a long-range charge-order would be present, an arbitrary weak interaction between third-nearest neighbors ($W_3 \neq 0$) is sufficient. $W_3 < 0$ gives long-range order of the four-sublattice type for SC and BCC lattices (for $W_3 > 0$ 4×2 (eight-sublattice) orderings need to be considered) [61, 62]. In a case of 1D chain the long-range order appears for $W_3 > 0$, whereas $W_3 < 0$ stabilizes eight-sublattice orderings.

The phases with single-occupied sites are infinitely (macroscopically) degenerate with respect to spin degrees

of freedom and thus the model considered does not exhibit any magnetic order in any dimension.

Similarly as the Ising model with short-range interactions, model (1) considered on one-dimensional lattice does not exhibit long-range order at any $T > 0$ for any model parameters [38, 48]. For the two-dimensional lattice the order above the ground state CBO, STO and FCBO, regions (i.e., nonfilled regions in Fig. 2) would occur for fixed $\bar{\mu}$ [40, 41, 63–66]. At incommensurate fillings one should expect the order at $T > 0$ also in the FCBO_B and FCBO_E regions as well as in regions where the PS states are stable at $T = 0$. For $d \geq 3$ the order should be present at small $T > 0$ for all model parameters (excluding those for which the NO phase occurs at $T = 0$).

IV. FINAL REMARKS

We considered the zero-bandwidth extended Hubbard model taking into account longer-range (NN and NNN) interactions. It was found that such correlations give rise to four-sublattice solutions for $W_2 > 0$ at the mean-field level (with exact treatment of the on-site term). We indicated that these new phases emerge at a given magnitude of the on-site interactions U . It was shown that the FNO phase is present for arbitrary values of U , and the FSTO phase occurs only for repulsive U , while the FCBO phase is limited by the $0 < U < W_1$ condition. For fixed electron concentration the system is highly degenerated, but arbitrary small temperature ($T > 0$) removes this degeneracy. We also show that not all phase transitions occurring at $T = 0$ remain first-order at finite temperatures. They are second-order ones at $T > 0$.

We discussed the influence of the lattice dimensionality d on the degeneracy of the ground state (for fixed μ). For the $d = 3$ lattice the results are in an agreement with the mean-field findings and finite degeneracy is present for arbitrary model parameters. In a case of lower dimensionalities ($d = 1, 2$) the appearance of the partial and full mixing of the elementary blocks gives rise to infinite degeneracy. We showed also that four-sublattice long-range order in low dimensions is suppressed (in the FNO and FSTO phases), but in the FCBO phase the long-range order remains.

Finally, let us note that in this work we analyzed the system neglecting the influence of the electron hopping term. It is known that finite hopping induces additional magnetic orderings [8, 67–70]. The other aspect related to quantum fluctuations introduced by the hopping is a metal-insulator transition. Basing on the results obtained for two sublattice assumption (for $W_2 = 0$) [6–9] one can expect that CBO and STO phases for $W_2 \neq 0$ should survive in a presence of such fluctuations. It is an open question whether other orderings (i.e., FNO, FCBO, and FSTO) will also remain (in insulating or metallic states). Although our system is simplified for this point, the results obtained here are exact solutions.

Therefore, they can be used to inspect the validity of approximations used to the more general models including single-electron hopping.

ACKNOWLEDGMENTS

The authors thank Anna Ciechan for very fruitful discussions. The authors acknowledge the support from the National Science Centre (NCN, Poland) under grants no. UMO-2014/15/B/ST3/03898 (K.J.K.), UMO-2016/21/D/ST3/03385 (K.J.K. and J.B.), UMO-2017/24/C/ST3/00276 (K.J.K.), and UMO-2016/20/S/ST3/00274 (A.P.).

Appendix A: The equivalent models

One can show (cf. e.g. Refs. [40, 43]) that model (1) is equivalent with the classical Blume-Capel model with spin $S = 1$ [71–74] in the external magnetic field, which has the following form

$$\hat{H}_{BC} = \Delta \sum_i \left(\tilde{S}_i^z \right)^2 + \frac{1}{2} \sum_{i,j} J_{ij} \tilde{S}_i^z \tilde{S}_j^z - H \sum_i \tilde{S}_i^z + C, \quad (\text{A1})$$

where $\Delta = \frac{1}{2}U + k_B T \ln(2)$ is temperature-dependent single-ion anisotropy, $J_{ij} = W_{ij}$, $H \equiv \bar{\mu} = \mu - U/2 - \sum_n z_n W_n$, $C = L(k_B T \ln(2) + \mu)$. For $U \rightarrow -\infty$ models (1) and (A1) are reduced to the standard $S = 1/2$ Ising model ($S_i^z = \pm 1$) [64–66, 75–77]. At $T = 0$ for $U = 0$ models (1) and (A1) are reduced to the $S = 1$ Ising model ($S_i^z = -1, 0, 1$). In Eq. (A1) we do not restrict the range of intersite interactions.

-
- [1] E. Wigner, “On the interaction of electrons in metals,” *Phys. Rev.* **46**, 1002–1011 (1934).
- [2] S. Robaszkiewicz, “The charge-ordered state in an extended Hubbard model,” *Phys. Status Sol. B* **59**, K63–K65 (1973).
- [3] R. Micnas, J. Ranninger, and S. Robaszkiewicz, “Superconductivity in narrow-band systems with local non-retarded attractive interactions,” *Rev. Mod. Phys.* **62**, 113–171 (1990).
- [4] R. Pietig, R. Bulla, and S. Blawid, “Reentrant charge order transition in the extended Hubbard model,” *Phys. Rev. Lett.* **82**, 4046–4049 (1999).
- [5] M. Aichhorn, H. G. Evertz, W. von der Linden, and M. Potthoff, “Charge ordering in extended Hubbard models: Variational cluster approach,” *Phys. Rev. B* **70**, 235107 (2004).
- [6] A. Amaricci, A. Camjayi, K. Haule, G. Kotliar, D. Tanasković, and V. Dobrosavljević, “Extended Hubbard model: Charge ordering and Wigner-Mott transition,” *Phys. Rev. B* **82**, 155102 (2010).
- [7] L. Huang, T. Ayrál, S. Biermann, and P. Werner, “Extended dynamical mean-field study of the Hubbard model with long-range interactions,” *Phys. Rev. B* **90**, 195114 (2014).
- [8] G. Giovannetti, R. Nourafkan, G. Kotliar, and M. Capone, “Correlation-driven electronic multiferroicity in TMTTF₂–X organic crystals,” *Phys. Rev. B* **91**, 125130 (2015).
- [9] K. J. Kapcia, S. Robaszkiewicz, M. Capone, and A. Amaricci, “Doping-driven metal-insulator transitions and charge orderings in the extended Hubbard model,” *Phys. Rev. B* **95**, 125112 (2017).
- [10] R. Comin, R. Sutarto, E. H. da Silva Neto, L. Chauviere, R. Liang, W. N. Hardy, D. A. Bonn, F. He, G. A. Sawatzky, and A. Damascelli, “Broken translational and rotational symmetry via charge stripe order in underdoped YBa₂Cu₃O_{6+y},” *Science* **347**, 1335–1339 (2015).
- [11] E. H. da Silva Neto, R. Comin, F. He, R. Sutarto, Y. Jiang, R. L. Greene, G. A. Sawatzky, and A. Damascelli, “Charge ordering in the electron-doped superconductor Nd_{2–x}Ce_xCuO₄,” *Science* **347**, 282–285 (2015).
- [12] D. Pelc, M. Vuckovic, H. J. Grafe, S. H. Baek, and M. Pozek, “Unconventional charge order in a Co-doped high-T_c superconductor,” *Nat. Commun.* **7**, 12775 (2016).
- [13] P. Cai, W. Ruan, Y. Peng, C. Ye, X. Li, Z. Hao, X. Zhou, D.-H. Lee, and Y. Wang, “Visualizing the evolution from the Mott insulator to a charge-ordered insulator in lightly doped cuprates,” *Nat. Phys.* **12**, 1047–1051 (2016).
- [14] P.-J. Hsu, J. Kuegel, J. Kemmer, F. P. Toldin, T. Mauerer, M. Vogt, F. Assaad, and M. Bode, “Co-existence of charge and ferromagnetic order in fcc Fe,” *Nat. Commun.* **7**, 10949 (2016).
- [15] S. Y. Park, A. Kumar, and K. M. Rabe, “Charge-order-induced ferroelectricity in LaVO₃/SrVO₃ superlattices,” *Phys. Rev. Lett.* **118**, 087602 (2017).
- [16] K. Yoshimi, H. Seo, S. Ishibashi, and Stuart E. Brown, “Tuning the magnetic dimensionality by charge ordering in the molecular TMTTF salts,” *Phys. Rev. Lett.* **108**, 096402 (2012).
- [17] B. A. Frandsen, E. S. Bozin, H. Hu, Y. Zhu, Y. Nozaki, H. Kageyama, Y. J. Uemura, W.-G. Yin, and S. J. L. Billinge, “Intra-unit-cell nematic charge order in the titanium-oxypnictide family of superconductors,” *Nat. Commun.* **5**, 5761 (2014).
- [18] A. M. Novello, M. Spera, A. Scarfato, A. Ubaldini, E. Giannini, D. R. Bowler, and Ch. Renner, “Stripe and short range order in the charge density wave of 1T–Cu_xTiSe₂,” *Phys. Rev. Lett.* **118**, 017002 (2017).
- [19] P. Bak and J. von Boehm, “Ising model with solitons, phasons, and “the devil’s staircase,”” *Phys. Rev. B* **21**, 5297–5308 (1980).
- [20] P. Bak and R. Bruinsma, “One-dimensional Ising model and the complete devil’s staircase,” *Phys. Rev. Lett.* **49**, 249–251 (1982).
- [21] P. Bak, “Commensurate phases, incommensurate phases and the devil’s staircase,” *Rep. Prog. Phys.* **45**, 587 (1982).

- [22] S. J. Lee, J.-R. Lee, and B. Kim, “Patterns of striped order in the classical lattice coulomb gas,” *Phys. Rev. Lett.* **88**, 025701 (2001).
- [23] L. Rademaker, Y. Pramudya, J. Zaanen, and V. Dobrosavljević, “Influence of long-range interactions on charge ordering phenomena on a square lattice,” *Phys. Rev. E* **88**, 032121 (2013).
- [24] M. B. Salamon and M. Jaime, “The physics of manganites: Structure and transport,” *Rev. Mod. Phys.* **73**, 583–628 (2001).
- [25] Z. Sun, Q. Wang, A. V. Fedorov, H. Zheng, J. F. Mitchell, and D. S. Dessau, “Localization of electrons due to orbitally ordered bi-stripes in the bilayer manganite $\text{La}_{2-2x}\text{Sr}_{1+2x}\text{Mn}_2\text{O}_7$ ($x \sim 0.59$),” *PNAS* **108**, 11799–11803 (2011).
- [26] E. C. Andrade and M. Vojta, “Disorder, cluster spin glass, and hourglass spectra in striped magnetic insulators,” *Phys. Rev. Lett.* **109**, 147201 (2012).
- [27] J. M. Tranquada, D. J. Buttrey, V. Sachan, and J. E. Lorenzo, “Simultaneous ordering of holes and spins in $\text{La}_2\text{NiO}_{4.125}$,” *Phys. Rev. Lett.* **73**, 1003–1006 (1994).
- [28] E. H. Lieb and F. Y. Wu, “Absence of mott transition in an exact solution of the short-range, one-band model in one dimension,” *Phys. Rev. Lett.* **20**, 1445–1448 (1968).
- [29] E. H. Lieb, “Two theorems on the Hubbard model,” *Phys. Rev. Lett.* **62**, 1201–1204 (1989).
- [30] A. Georges, G. Kotliar, W. Krauth, and M. J. Rozenberg, “Dynamical mean-field theory of strongly correlated fermion systems and the limit of infinite dimensions,” *Rev. Mod. Phys.* **68**, 13–125 (1996).
- [31] J. K. Freericks and R. Lemański, “Segregation and charge-density-wave order in the spinless Falicov-Kimball model,” *Phys. Rev. B* **61**, 13438–13444 (2000).
- [32] R. Lemański and K. Ziegler, “Gapless metallic charge-density-wave phase driven by strong electron correlations,” *Phys. Rev. B* **89**, 075104 (2014).
- [33] R. A. Bari, “Effects of short-range interactions on electron-charge ordering and lattice distortions in the localized state,” *Phys. Rev. B* **3**, 2662–2670 (1971).
- [34] G. Beni and P. Pincus, “Thermodynamics of an extended Hubbard model chain. I: Atomic limit for the half-filled band,” *Phys. Rev. B* **9**, 2963–2970 (1974).
- [35] R. S. Tu and T. A. Kaplan, “Effect of interatomic interactions on the zero-bandwidth Hubbard hamiltonian,” *Phys. Status Solidi B* **63**, 659–662 (1974).
- [36] F. Mancini, “Fermionic systems with charge correlations,” *EPL (Europhys. Lett.)* **70**, 485 (2005).
- [37] F. Mancini, “The extended Hubbard model in the ionic limit,” *Eur. Phys. J. B* **47**, 527–540 (2005).
- [38] F. Mancini and F. P. Mancini, “One-dimensional extended Hubbard model in the atomic limit,” *Phys. Rev. E* **77**, 061120 (2008).
- [39] F. Mancini and F. P. Mancini, “Extended Hubbard model in the presence of a magnetic field,” *Eur. Phys. J. B* **68**, 341–351 (2009).
- [40] J. Jędrzejewski, “Phase diagrams of extended Hubbard models in the atomic limit,” *Physica A* **205**, 702–717 (1994).
- [41] C. Borgs, J. Jędrzejewski, and R. Kotecký, “The staggered charge-order phase of the extended Hubbard model in the atomic limit,” *J. Phys. A: Math. Gen.* **29**, 733–747 (1996).
- [42] J. Fröhlich, L. Rey-Bellet, and D. Ueltschi, “Quantum lattice models at intermediate temperature,” *Comm. Math. Phys.* **224**, 33–63 (2001).
- [43] G. Pawłowski, “Charge orderings in the atomic limit of the extended Hubbard model,” *Eur. Phys. J. B* **53**, 471–479 (2006).
- [44] G. Ganzenmüller and G. Pawłowski, “Flat histogram Monte Carlo sampling for mechanical variables and conjugate thermodynamic fields with example applications to strongly correlated electronic systems,” *Phys. Rev. E* **78**, 036703 (2008).
- [45] F. Mancini, F. P. Mancini, and A. Naddeo, “Role of the attractive intersite interaction in the extended Hubbard model,” *Eur. Phys. J. B* **68**, 309–315 (2009).
- [46] F. Mancini and F. P. Mancini, “Different orderings in the narrow-band limit of the extended Hubbard model on the Bethe lattice,” *Eur. Phys. J. B* **73**, 581–595 (2010).
- [47] S. Robaszkiewicz and T. Kostyrko, “The influence of electron-electron and electron-phonon interactions on electron charge orderings in quasi-one-dimensional systems,” *Physica B+C* **112**, 389–405 (1982).
- [48] F. Mancini, E. Plekhanov, and G. Sica, “Exact solution of the 1D Hubbard model with NN and NNN interactions in the narrow-band limit,” *Eur. Phys. J. B* **86**, 408 (2013).
- [49] R. Micnas, S. Robaszkiewicz, and K. A. Chao, “Multicritical behavior of the extended Hubbard model in the zero-bandwidth limit,” *Phys. Rev. B* **29**, 2784–2789 (1984).
- [50] R. J. Bursill and C. J. Thompson, “Variational bounds for lattice fermion models II. Extended Hubbard model in the atomic limit,” *J. Phys. A: Math. Gen.* **26**, 4497–4511 (1993).
- [51] K. Kapcia and S. Robaszkiewicz, “The effects of the next-nearest-neighbour density-density interaction in the atomic limit of the extended Hubbard model,” *J. Phys.: Condens. Matter* **23**, 105601 (2011).
- [52] K. J. Kapcia and S. Robaszkiewicz, “On the phase diagram of the extended Hubbard model with intersite density-density interactions in the atomic limit,” *Physica A* **461**, 487–497 (2016).
- [53] K. J. Kapcia, J. Barański, S. Robaszkiewicz, and A. Ptok, “Various charge-ordered states in the extended Hubbard model with on-site attraction in the zero-bandwidth limit,” *J. Supercond. Nov. Magn.* **30**, 109–115 (2017).
- [54] E. Müller-Hartmann, “Correlated fermions on a lattice in high dimensions,” *Z. Phys. B* **74**, 507–512 (1989).
- [55] P. A. Pearce and C. J. Thompson, “The anisotropic Heisenberg model in the long-range interaction limit,” *Comm. Math. Phys.* **41**, 191–201 (1975).
- [56] P. A. Pearce and C. J. Thompson, “The high density limit for lattice spin models,” *Comm. Math. Phys.* **58**, 131–138 (1978).
- [57] S. A. Pirogov and Ya. G. Sinai, “Phase diagrams of classical lattice systems,” *Theor. Math. Phys.* **25**, 1185–1192 (1975).
- [58] S. A. Pirogov and Ya. G. Sinai, “Phase diagrams of classical lattice systems. Continuation,” *Theor. Math. Phys.* **26**, 39–49 (1976).
- [59] J. Fröhlich, R. Israel, E. H. Lieb, and B. Simon, “Phase transitions and reflection positivity. I. General theory and long range lattice models,” *Comm. Math. Phys.* **62**, 1–34 (1978).
- [60] J. Fröhlich, R. B. Israel, E. H. Lieb, and B. Simon, “Phase transitions and reflection positivity. II. Lattice systems with short-range and coulomb interactions,” *J.*

- Stat. Phys.* **22**, 297–347 (1980).
- [61] D. P. Landau and K. Binder, “Phase diagrams and critical behavior of Ising square lattices with nearest-, next-nearest-, and third-nearest-neighbor couplings,” *Phys. Rev. B* **31**, 5946–5953 (1985).
- [62] R. M. Liu, W. Z. Zhuo, S. Dong, X. B. Lu, X. S. Gao, M. H. Qin, and J.-M. Liu, “Role of further-neighbor interactions in modulating the critical behavior of the Ising model with frustration,” *Phys. Rev. E* **93**, 032114 (2016).
- [63] J. Jędrzejewski, “On the phase diagram of the extended Hubbard model,” *Z. Phys. B* **59**, 325–332 (1985).
- [64] K. Binder and D. P. Landau, “Phase diagrams and critical behavior in Ising square lattices with nearest- and next-nearest-neighbor interactions,” *Phys. Rev. B* **21**, 1941–1962 (1980).
- [65] R. A. dos Anjos, J. R. Viana, J. R. de Sousa, and J. A. Plascak, “Three-dimensional Ising model with nearest- and next-nearest-neighbor interactions,” *Phys. Rev. E* **76**, 022103 (2007).
- [66] A. Bobák, T. Lučivjanský, M. Borovský, and M. Žukovič, “Phase transitions in a frustrated Ising antiferromagnet on a square lattice,” *Phys. Rev. E* **91**, 032145 (2015).
- [67] Y. Nagaoka, “Ferromagnetism in a narrow, almost half-filled s band,” *Phys. Rev.* **147**, 392–405 (1966).
- [68] K. A. Chao, J. Spalek, and A. M. Oleś, “Kinetic exchange interaction in a narrow s -band,” *J. Phys. C* **10**, L271–L276 (1977).
- [69] K. A. Chao, J. Spalek, and A. M. Oleś, “Canonical perturbation expansion of the Hubbard model,” *Phys. Rev. B* **18**, 3453–3465 (1978).
- [70] K. Penc and F. Mila, “Phase diagram of the one-dimensional extended Hubbard model with attractive and/or repulsive interactions at quarter filling,” *Phys. Rev. B* **49**, 9670–9678 (1994).
- [71] M. Blume, “Theory of the first-order magnetic phase change in UO_2 ,” *Phys. Rev.* **141**, 517–524 (1966).
- [72] H. W. Capel, “On the possibility of first-order phase transitions in Ising systems of triplet ions with zero-field splitting,” *Physica* **32**, 966–988 (1966).
- [73] M. Blume, V. J. Emery, and R. B. Griffiths, “Ising model for the λ transition and phase separation in He^3 - He^4 mixtures,” *Phys. Rev. A* **4**, 1071–1077 (1971).
- [74] M. Bادهداه, S. Bekhechi, A. Benyoussef, and M. Touzani, “Phase transition in the Blume-Capel model with second neighbour interaction,” *Eur. Phys. J. B* **4**, 431–440 (1998).
- [75] K. Yamada and J. Kanamori, “Magnetization process in antiferromagnets with a strong uniaxial anisotropy energy,” *Prog. Theor. Phys.* **38**, 541–550 (1967).
- [76] S. Katsura and S. Fujimori, “Magnetization process and the critical field of the Ising model with first- and second-neighbour interactions,” *J. Phys. C: Solid State Phys.* **7**, 2506–2520 (1974).
- [77] J. M. Kincaid and E. G. D. Cohen, “Phase diagrams of liquid helium mixtures and metamagnets: Experiment and mean field theory,” *Phys. Rep.* **22**, 57–143 (1975).